Direct detection of dynamical dark matter

Keith R. Dienes, Jason Kumar, and Brooks Thomas

Direct Detection of Dynamical Dark Matter

Keith R. Dienes[1,2,3*], Jason Kumar[4†], Brooks Thomas[4‡]

[1] *Physics Division, National Science Foundation, Arlington, VA 22230 USA*
[2] *Department of Physics, University of Maryland, College Park, MD 20742 USA*
[3] *Department of Physics, University of Arizona, Tucson, AZ 85721 USA*
[4] *Department of Physics, University of Hawaii, Honolulu, HI 96822 USA*

Dynamical dark matter (DDM) is an alternative framework for dark-matter physics in which the dark-matter candidate is an ensemble of constituent fields with differing masses, lifetimes, and cosmological abundances. In this framework, it is the balancing of these quantities against each other across the ensemble as a whole which ensures phenomenological viability. In this paper, we examine the prospects for the direct detection of a DDM ensemble. In particular, we study the constraints imposed by current limits from direct-detection experiments on the parameter space of DDM models, and we assess the prospects for detecting such an ensemble and distinguishing it from traditional dark-matter candidates on the basis of data from the next generation of direct-detection experiments. For concreteness, we focus primarily on the case in which elastic scattering via spin-independent interactions dominates the interaction rate between atomic nuclei and the constituent particles of the ensemble. We also briefly discuss the effects of modifying these assumptions.

I. INTRODUCTION

Dynamical dark matter (DDM) [1, 2] has recently been advanced as an alternative framework for dark-matter physics. In this framework, the usual assumption of dark-matter stability is replaced by a balancing between lifetimes and cosmological abundances across a vast ensemble of particles which collectively constitute the dark matter. Within this framework, the dark-matter candidate is the full ensemble itself — a collective entity which cannot be characterized in terms of a single, well-defined mass, lifetime, or set of interaction cross-sections with visible matter. As a result, cosmological quantities such as the total relic abundance $\Omega_{\rm tot}$ of the ensemble, its composition, and its equation of state are time-dependent (*i.e.*, dynamical) and evolve throughout the history of the universe. Moreover, for this same reason, DDM ensembles also give rise to a variety of distinctive experimental signatures which serve to distinguish them from traditional dark-matter candidates. A number of phenomenological and cosmological consequences to which DDM ensembles can give rise were presented in Refs. [2, 3], along with the bounds such effects imply on the parameter space of an explicit model within the general DDM framework. DDM ensembles can also give rise to characteristic signatures at colliders [4], including distinctive imprints on the kinematic distributions of the Standard-Model (SM) particles produced in conjunction with the dark-sector fields.

In this paper, we examine the prospects for the direct detection of DDM ensembles via their interactions with atomic nuclei — a detection strategy [5] which has come to play an increasingly central role in the phenomenology of most proposed dark-matter candidates (for reviews, see, *e.g.*, Ref. [6]). Indeed, conclusive evidence of nuclear recoils induced by the scattering of particles in the dark-matter halo would provide the most unambiguous and compelling signal — and moreover the only non-gravitational evidence — for particle dark matter to date. Data from the current generation of direct-detection experiments has already placed stringent constraints on many models of the dark sector, and the detection prospects have been investigated for a variety of traditional dark-matter candidates at next generation of such experiments. Studies in the context of particular multi-component models of the dark sector have also been performed [7, 8].

Here, we shall demonstrate that DDM ensembles can give rise to distinctive features in the recoil-energy spectra observed at direct-detection experiments, and that these features can serve to distinguish DDM ensembles from traditional dark-matter candidates. These features include resolvable kinks in the recoil energy spectra, as well as characteristic shapes which are difficult to realize within the context of traditional models — particularly under standard astrophysical assumptions. As we shall demonstrate, these features should be distinguishable for a broad range of DDM scenarios at the next generation of direct-detection experiments. Of course, the potential for differentiation within the appropriate limiting regimes of DDM parameter space accords with those obtained in previous studies of two-component models [8]. However, as we shall demonstrate, the assumption of a full DDM ensemble as our

dark-matter candidate leads to many distinctive features which emerge in significant regions of parameter space and which transcend those which arise for models with only a few dark-sector particles.

This paper is organized as follows. In Sect. II, we review the general aspects of dark-matter direct detection. We discuss how considerations related to particle physics, nuclear physics, and astrophysics impact both the differential and total rate for the inelastic scattering of dark-matter particles with atomic nuclei, and examine the properties of the recoil-energy spectra associated with from traditional dark-matter candidates. In Sect. III, by contrast, we investigate how these results are modified when the dark-matter candidate is a DDM ensemble, and we compare the resulting recoil-energy spectra to those obtained in traditional dark-matter models. In Sect. IV, we derive a set of constraints on the parameter space of DDM models from current direct-detection data, and in Sect. V, we discuss the prospects for obtaining evidence of DDM ensembles at the next generation of direct-detection experiments and for distinguishing such ensembles from traditional dark-matter candidates. Finally, in Sect. VI, we summarize our results and discuss possible directions for future study.

II.   DIRECT DETECTION: PRELIMINARIES

We begin our study by briefly reviewing the situation in which a traditional dark-matter candidate χ with a mass m_χ scatters off a collection of atomic nuclei. In general, the differential rate (per unit mass of detector material) for the scattering of such a dark-matter candidate off a collection of atomic nuclei can be written in the form [6]

$$\frac{dR}{dE_R} \;=\; \frac{\sigma_{N\chi}^{(0)}\rho_\chi^{\rm loc}}{2m_\chi\mu_{N\chi}^2}F^2(E_R)I_\chi(E_R) \;, \tag{2.1}$$

where E_R is the recoil energy of the scattered nucleus in the reference frame of the detector, $\sigma_{N\chi}^{(0)}$ is the χ-nucleus scattering cross-section at zero momentum transfer, $\rho_\chi^{\rm loc}$ is the *local* energy density of χ, $F(E_R)$ is a nuclear form factor, m_N is the mass of the scattered nucleus N, $\mu_{N\chi} \equiv m_\chi m_N/(m_\chi + m_N)$ is the reduced mass of the χ-nucleus system, and $I_\chi(E_R)$ is the mean inverse speed of χ in the dark-matter halo for a given E_R. This mean inverse speed, which encodes the relevant information about the halo-velocity distribution of χ, is given by

$$I_\chi(E_R) \;\equiv\; \int_{v>v_{\rm min}} \frac{\mathcal{F}_\chi(\vec{v})}{v}d^3v \;, \tag{2.2}$$

where $\mathcal{F}_\chi(\vec{v})$ denotes the distribution of the detector-frame velocities $\vec{v}$ of the χ in the local dark-matter halo and where $v \equiv |\vec{v}|$. The lower limit $v_{\rm min}$ on v follows from the condition that only those χ with velocities in excess of the kinematic threshold for non-relativistic scattering

$$v_{\rm min} \;\equiv\; \sqrt{\frac{E_R m_N}{2\mu_{N\chi}^2}} \;, \tag{2.3}$$

can contribute to the scattering rate. Moreover, the halo-velocity distribution $\mathcal{F}_\chi(\vec{v})$ itself is truncated at $|\vec{v}+\vec{v}_e| < v_{\rm esc}$, where $\vec{v}_e$ is the velocity of the earth with respect to the dark-matter halo, and where $v_{\rm esc}$ is the galactic escape velocity. Indeed, any dark-matter particle with a speed in excess of $v_{\rm esc}$ in the rest frame of the dark-matter halo would likely have escaped from the galaxy long ago.

One of the primary challenges in interpreting direct-detection data is that substantial uncertainties exist in many of the quantities appearing in Eq. (2.1). It is therefore necessary for one to make certain assumptions about the properties of the dark-matter halo, the nuclear form factor, *etc.*, in order to make concrete predictions regarding the detection prospects for any given theory of dark matter. Consequently, in this paper, we adopt a "standard benchmark" set of well-motivated assumptions concerning the relevant quantities in Eq. (2.1).

The first class of assumptions which define our standard benchmark are those related to particle physics. In particular, we take the dark sector to comprise a traditional dark-matter particle χ which scatters purely elastically off nuclei. Moreover, spin-independent scattering is assumed to dominate the total scattering rate. It follows that $\sigma_{N\chi}^{(0)}$ may be written in the form

$$\sigma_{N\chi}^{(0)} \;=\; \frac{4\mu_{Nj}^2}{\pi}\big[Zf_{p\chi} + (A-Z)f_{n\chi}\big]^2 \;, \tag{2.4}$$

where $f_{p\chi}$ and $f_{n\chi}$ are the respective effective couplings of χ to the proton and neutron, Z is the atomic number of the nucleus in question, and A is its atomic mass. In addition, the interactions between χ and nucleons are taken to

be isospin-conserving, in the sense that $f_{p\chi} = f_{n\chi}$; hence Eq. (2.4) reduces to

$$\sigma_{N\chi}^{(0)} = \frac{4\mu_{N\chi}^2}{\pi} f_{n\chi}^2 A^2 . \tag{2.5}$$

Similarly, it is also useful to define the spin-independent cross-section *per nucleon* at zero-momentum transfer:

$$\sigma_{n\chi}^{(\mathrm{SI})} \equiv \frac{4\mu_{n\chi}^2}{\pi} f_{n\chi}^2 = \sigma_{N\chi}^{(0)} \frac{\mu_{n\chi}^2}{\mu_{N\chi}^2 A^2} , \tag{2.6}$$

where $\mu_{n\chi}$ is the reduced mass of the χ-nucleon system. This quantity has the advantage of being essentially independent of the properties of the target material, and therefore useful for comparing data from different experiments.

The second class of assumptions which define our standard benchmark are those related to the astrophysics of the dark-matter halo. In particular, the local dark-matter density is taken to be $\rho_{\mathrm{tot}}^{\mathrm{loc}} \approx 0.3$ GeV/cm^3 and the velocity distribution of particles in the dark-matter halo is taken to be Maxwellian. From the latter assumption, it follows that the integral over halo velocities in Eq. (2.2) is [9, 10]

$$I_\chi(E_R) = \frac{k}{2v_e} \times \begin{cases} \mathrm{erf}\left(\dfrac{v_{\min} + v_e}{v_0}\right) - \mathrm{erf}\left(\dfrac{v_{\min} - v_e}{v_0}\right) - \dfrac{4v_e}{v_0\sqrt{\pi}} e^{-v_{\mathrm{esc}}^2/v_0^2} & v_{\min} \leq v_{\mathrm{esc}} - v_e \\[3mm] \mathrm{erf}\left(\dfrac{v_{\mathrm{esc}}}{v_0}\right) - \mathrm{erf}\left(\dfrac{v_{\min} - v_e}{v_0}\right) - \dfrac{2(v_{\mathrm{esc}} + v_e - v_{\min})}{v_0\sqrt{\pi}} e^{-v_{\mathrm{esc}}^2/v_0^2} & v_{\mathrm{esc}} - v_e < v_{\min} \leq v_{\mathrm{esc}} + v_e \\[3mm] 0 & v_{\min} > v_{\mathrm{esc}} + v_e \end{cases} \tag{2.7}$$

where $v_0 \approx 220$ km/s is the local circular velocity and

$$k \equiv \left[\mathrm{erf}\left(\frac{v_{\mathrm{esc}}}{v_0}\right) - \frac{2v_{\mathrm{esc}}}{v_0\sqrt{\pi}} e^{-v_{\mathrm{esc}}^2/v_0^2} \right]^{-1} \tag{2.8}$$

is a coefficient which is independent of both time and m_χ. By contrast, v_e is time-dependent and modulates annually due to the revolution of the Earth around the sun. However, in this paper, we focus primarily on the time-averaged scattering rate observed at a given experiment. We therefore approximate the expression in Eq. (2.7) by replacing v_e with its annual average $\langle v_e \rangle \approx 1.05\, v_0$ in what follows. Finally, the galactic escape velocity is taken to be $v_{\mathrm{esc}} \approx 540$ km/s, in accord with the results obtained from the RAVE survey [11].

The third class of assumptions which define our standard benchmark are those related to nuclear physics. These assumptions are collectively embodied by the nuclear form factor $F(E_R)$. In our standard benchmark, this form factor is taken to have the Helm functional form [12]

$$F(E_R) = \frac{3J_1(\sqrt{2m_N E_R} R_1)}{\sqrt{2m_N E_R} R_1} e^{-m_N E_R s^2} , \tag{2.9}$$

where $J_1(x)$ denotes the spherical Bessel function, $s \approx 0.9$ fm is an empirically-determined length scale, and $R_1 \equiv \sqrt{R^2 - 5s^2}$, with $R \equiv (1.2 \text{ fm}) \times A^{1/3}$. Note that there exist particular values of E_R at which $F(E_R)$ vanishes in this form-factor model (due to the zeroes of the Bessel function), in the vicinity of which results derived using Eq. (2.9) are unreliable. However, turns out that all such values of E_R will lie well outside the range relevant for our analysis.

Of course, deviations from this standard benchmark can have a potentially significant impact on recoil-energy spectra. For example, the effects of unorthodox coupling structures [13, 14], more complicated velocity distributions [15], different values of the local dark-matter energy density [16], and alternative form-factor models [17] have all been investigated in the literature. In this paper, however, we shall concentrate on the effects that arise when a traditional dark-matter candidate is replaced by a DDM ensemble and hold all other aspects our standard benchmark fixed.

The standard benchmark described above already leads to characteristic spectra for traditional dark-matter candidates. In Fig. 1, we display a set of recoil-energy spectra associated with the spin-independent scattering of such dark-matter candidates off xenon nuclei (left panel) and germanium nuclei (right panel) for our standard benchmark. In each panel, the curves shown correspond to several different values of m_χ, and each of these curves is normalized such that $\sigma_{N\chi}^{(0)} = 1$ pb.

The shapes of the curves shown in Fig. 1 are determined primarily by two physical effects which suppress the differential event rate at large E_R. One of these effects stems from the distribution of particle velocities in the dark-matter halo. Since $\mathcal{F}(\vec{v})$ falls off exponentially at velocities above $|\vec{v} + \vec{v}_e| \sim v_0$, the recoil-energy spectra likewise
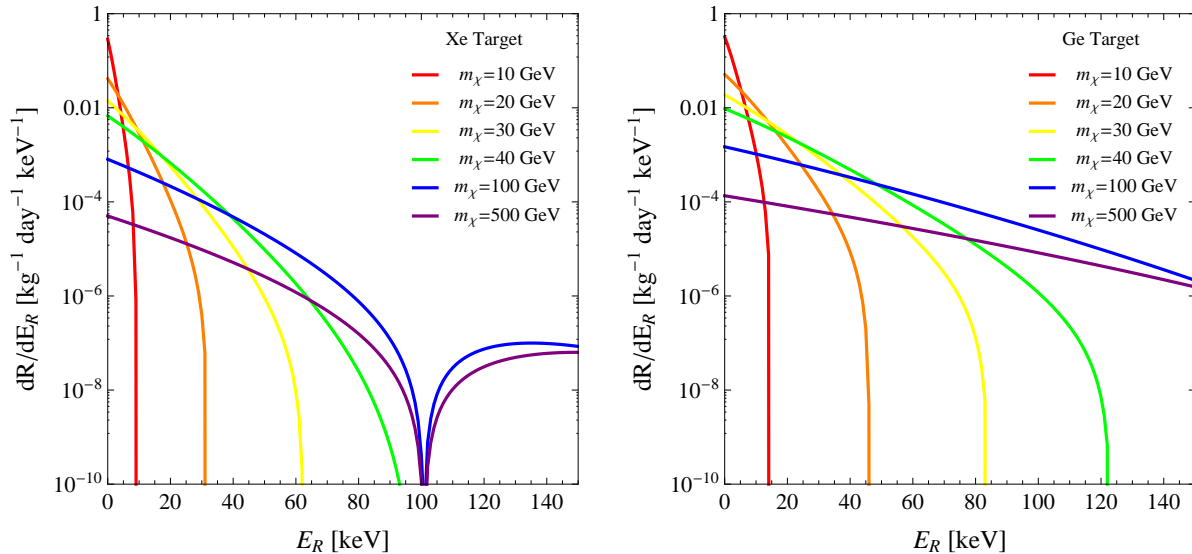
FIG. 1: A representative set of recoil-energy spectra obtained for a traditional dark-matter candidate χ with a mass m_χ scattering off a xenon target (left panel) and a germanium target (right panel).

experience a similar suppression above $E_R \sim 2(v_0 + v_e)^2 \mu_{N\chi}^2 / m_N$. Moreover, these spectra are also truncated at $E_R \sim 2(v_{\rm esc} + v_e)^2 \mu_{N\chi}^2 / m_N$ as a result of the galactic escape velocity. These effects are particularly important for $m_\chi \lesssim 40$ GeV and become increasingly pronounced as m_χ decreases. Indeed, we will see in Sect. III that these effects turn out to play a critical role in the direct-detection phenomenology of DDM ensembles, precisely because they are sensitive to m_χ.

The other effect which plays a significant role in determining the shape of the recoil-energy spectra shown in Fig. 1 has its origin in nuclear physics. As is evident from Eq. (2.9), the nuclear form factor also suppresses the differential event rate for large E_R. This suppression is particularly acute for heavier nuclei such as xenon ($A \approx 131$), and considerably less so for lighter nuclei such as germanium ($A \approx 73$). Note, however, that this effect is independent of m_χ and depends only on E_R and the properties of the target material. Note also that the dip in the recoil-energy spectra displayed in the left panel of Fig. 1 around $E_R \sim 100$ keV corresponds to the first zero of $F(E_R)$ in Eq. (2.9). As noted above, this turns out to lie well outside the range of E_R values relevant for this analysis.

We see, then, that there are qualitatively two distinct regimes which describe the differing behaviors of the resulting recoil-energy spectra. In the "low-mass regime," these spectra are steeply falling and highly sensitive to m_χ. By contrast, in the "high-mass regime," these curves fall more slowly and are less sensitive to m_χ. As we shall see in Sect. V, this distinction will ultimately play a critical role in our analysis.

III. DIRECT DETECTION OF DDM ENSEMBLES

Let us now examine how the results obtained in Sect. II are modified in the case in which the traditional dark-matter candidate is replaced by a DDM ensemble, with all of the other defining characteristics of our standard benchmark held fixed. As discussed in Refs. [1, 2], dynamical dark matter is a new framework for dark-matter physics in which the notion of stability is replaced by a delicate balancing between lifetimes and abundances across an ensemble of individual dark-matter components. As such, this framework represents the most general possible dark-matter sector that can be imagined while still satisfying astrophysical and cosmological bounds. Furthermore, as discussed in Ref. [1], dynamical dark matter arises naturally in certain theories involving extra spacetime dimensions, and also in certain limits of string theory. It is therefore important to consider how the direct-detection phenomenology of DDM ensembles differs from that of traditional dark-matter candidates. Indeed, such a study can be viewed as complementary to the collider analysis performed in Ref. [4].

From a direct-detection standpoint, the most salient difference between a DDM ensemble and a traditional dark-matter candidate is that by definition, a DDM ensemble comprises a vast number of constituent fields χ_j, each with a mass m_j and local energy density $\rho_j^{\rm loc}$. In general, since multiple states are present in the dark sector, both elastic processes of the form $\chi_j N \to \chi_j N$ and inelastic scattering processes of the form $\chi_j N \to \chi_k N$, with $j \neq k$, can contribute to the total χ_j-nucleon scattering rate. In this paper, in accord with the assumptions underlying

our standard picture of dark-matter physics, we focus primarily on the case in which elastic scattering provides the dominant contribution to the total scattering rate for each χ_j. (This occurs generically, for example, in situations in which the mass-splittings between all pairs of constituent particles in the ensemble substantially exceed 100 keV). In this case, each χ_j also possesses a well-defined effective spin-independent coupling f_{nj} to nucleons, and consequently a well-defined spin-independent cross-section per nucleon $\sigma_{n\chi}^{(\mathrm{SI})} \equiv 4\mu_{nj}^2 f_{nj}^2/\pi$. The total differential event rate at a given detector is obtained by summing over the contributions from each χ_j, each of which is given by an expression analogous to Eq. (2.1). Thus, for an arbitrary DDM ensemble, this total differential event rate takes the form

$$\frac{dR}{dE_R} = \sum_j \frac{\sigma_{Nj}^{(0)} \rho_j^{\mathrm{loc}}}{2m_j \mu_{Nj}^2} F^2(E_R) I_j(E_R) \;, \tag{3.1}$$

subject to the constraint $\sum_j \rho_j^{\mathrm{loc}} = \rho_{\mathrm{tot}}^{\mathrm{loc}}$. Note that the nuclear form factor depends only on E_R and not on the properties of the constituent particle χ_j. By contrast, the integral over halo velocities depends non-trivially on m_j through the kinematic threshold velocity

$$v_{\mathrm{min}}^{(j)} \equiv \sqrt{\frac{E_R m_N}{2\mu_{Nj}^2}} \;. \tag{3.2}$$

Note that this remains true even in the case we consider here, in which the velocity distributions for all χ_j are taken to be essentially identical.

The cosmology of DDM models is principally described by two characteristic quantities [1]. The first of these is the collective (present-day) relic abundance Ω_{tot} of the full DDM ensemble, which is simply a sum of the individual abundances Ω_j of the χ_j. The second quantity is

$$\eta \equiv 1 - \frac{\Omega_0}{\Omega_{\mathrm{tot}}} \tag{3.3}$$

where $\Omega_0 \equiv \max\{\Omega_j\}$; this helps to characterize the distribution of the Ω_j across the ensemble, and in particular represents the fraction of Ω_{tot} collectively provided by all but the most abundant constituent. Thus $\eta = 0$ effectively corresponds to the case of a traditional dark-matter candidate, while $\eta \sim \mathcal{O}(1)$ indicates that the full ensemble is contributing non-trivially to Ω_{tot}.

In general, the *local* energy densities ρ_j^{loc} of the χ_j — which play a crucial role in direct detection — need not have any relation to their *cosmological* abundances Ω_j. However, in typical cosmological models, the local energy density of any particular χ_j is approximately proportional to its cosmological abundance — *i.e.*, $\rho_j^{\mathrm{loc}}/\rho_{\mathrm{tot}}^{\mathrm{loc}} \approx \Omega_j/\Omega_{\mathrm{tot}}$. Furthermore, we assume that $\Omega_{\mathrm{tot}} \approx \Omega_{\mathrm{CDM}}$, so that the DDM ensemble contributes essentially the entirety of the cold-dark-matter relic abundance $\Omega_{\mathrm{CDM}} h^2 \approx 0.1131 \pm 0.0034$ determined by WMAP [18]. Under these assumptions, the differential event rate in Eq. (3.1) may be written in the form

$$\frac{dR}{dE_R} = \frac{2f_{n0}^2 \rho_{\mathrm{tot}}^{\mathrm{loc}} A^2}{\pi m_0}(1-\eta) F^2(E_R) \sum_j \left(\frac{\Omega_j m_0 f_{nj}^2}{\Omega_0 m_j f_{n0}^2}\right) I_j(E_R) \;, \tag{3.4}$$

where m_0 and f_{n0} respectively denote the mass and effective coupling coefficient of the most abundant state χ_0 in the ensemble.

For concreteness, we examine the direct-detection phenomenology of DDM ensembles in the context of a simplified DDM model. In this model χ_0 is identified with the lightest state in the ensemble, and the mass spectrum of the χ_j takes the form

$$m_j = m_0 + j^\delta \Delta m \tag{3.5}$$

with $\Delta m > 0$ and $\delta > 0$, so that the χ_j are labeled in order of increasing mass. Moreover, in this model Ω_j and f_{nj} are each assumed to exhibit power-law scaling with m_j across the ensemble, so that these quantities may be written in the form

$$\Omega_j = \Omega_0 \left(\frac{m_j}{m_0}\right)^\alpha$$

$$f_{nj} = f_{n0} \left(\frac{m_j}{m_0}\right)^\beta \;, \tag{3.6}$$

where α and β are general power-law exponents. Note that scaling relations of this form emerge naturally in many realistic DDM scenarios [1, 2, 4]. Also note that the direct-detection phenomenology of DDM ensembles depends on the present-day values of the Ω_j and not how these values have evolved in the past. Thus the decay widths of the χ_j, although crucial for the balancing of lifetimes against abundances within the DDM framework [1], play no role in direct detection.

For the purposes of direct detection, our simplified DDM ensemble is therefore characterized by two groups of parameters: those (namely m_0, Ω_0, and f_{n0}) which describe the properties of the most abundant state in the ensemble and which would also be necessary in any traditional dark-matter model, and those (namely Δm and the scaling exponents α, β, and δ) which describe how this information extends throughout the entire ensemble. This is therefore a very compact yet flexible formalism for exploring the ramifications of having an entire DDM ensemble as our dark-matter candidate. However, the WMAP constraint on $\Omega_{\rm tot}$ fixes one of these parameters (most conveniently Ω_0). Thus, the recoil-energy spectra to which our simplified DDM model gives rise are completely determined by α, β, δ, m_0, Δm, and f_{n0} (or equivalently $\sigma_{n0}^{\rm (SI)}$). Note also that the last of these parameters determines the normalization of the recoil-energy spectrum (i.e., the total event rate), but has no effect on the *shape* of that spectrum.

Given the scaling relations in Eqs. (3.5) and (3.6), it is straightforward to rewrite the expressions for $\Omega_{\rm tot}$ and η, as well as the differential event rate dR/dE_R, in terms of these parameters. Indeed, in the context of our simplified DDM model, the present-day values of $\Omega_{\rm tot}$ and η are given by

$$\Omega_{\rm tot} = \Omega_0 \sum_j \left(1 + j^\delta \frac{\Delta m}{m_0}\right)^\alpha$$

$$\eta = 1 - \left[\sum_j \left(1 + j^\delta \frac{\Delta m}{m_0}\right)^\alpha\right]^{-1}. \tag{3.7}$$

From a DDM perspective, our primary interest is in situations in which the number of constituent particles in the dark-matter ensemble is taken to be large. For this reason, we restrict our discussion to cases in which the sums in Eq. (3.7) are convergent even in the limit in which $j \to \infty$. Imposing this requirement restricts the purview of our analysis to cases in which the condition $\alpha\delta < -1$ is satisfied. Likewise, the expression in Eq. (3.4) for the differential event rate reduces to

$$\frac{dR}{dE_R} = \frac{2f_{n0}^2 \rho_{\rm tot}^{\rm loc} A^2}{\pi m_0}(1 - \eta)F^2(E_R) \sum_j I_j(E_R)\left(1 + j^\delta \frac{\Delta m}{m_0}\right)^{\alpha + 2\beta - 1}. \tag{3.8}$$
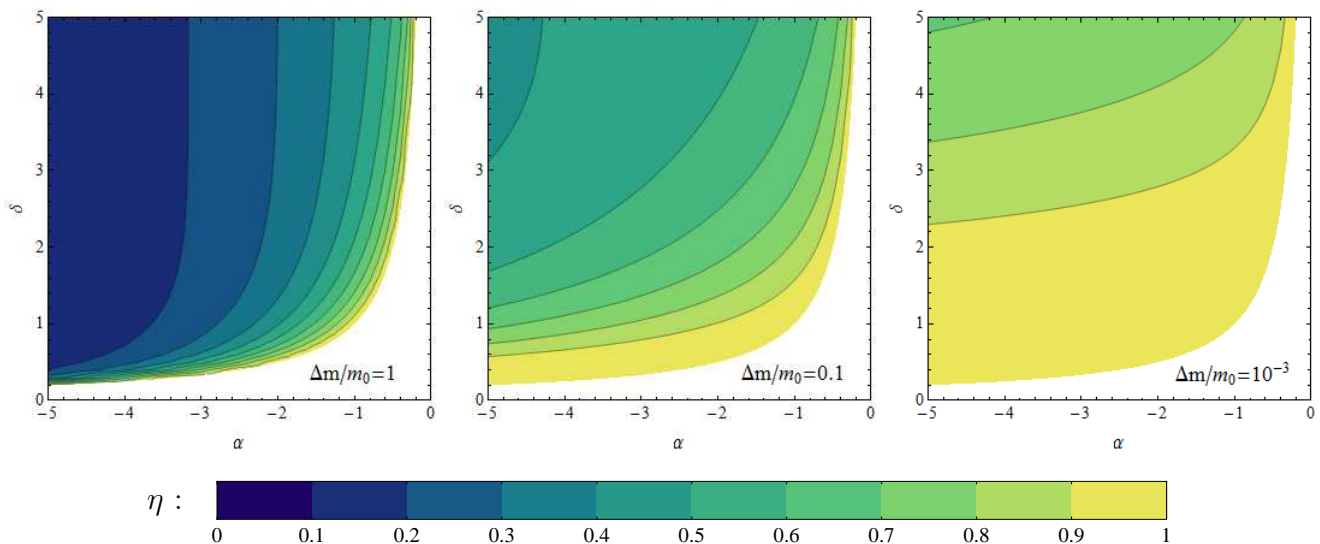

FIG. 2: Contours of η as a function of the scaling coefficients α and δ, derived under the assumption that $\Omega_{\rm tot} \approx \Omega_{\rm CDM}$. The left, center, and right panels show results for $\Delta m/m_0 = \{1, 0.1, 10^{-3}\}$, respectively. Note that as $\delta m/m_0 \to 0$ for fixed α and δ, we see that $\eta \to 1$ and the full ensemble provides a increasingly significant contribution to $\Omega_{\rm tot}$.

In Fig. 2, we provide a series of contour plots illustrating the dependence of η on the scaling coefficients α and δ in our simplified DDM model. The left, center, and right panels of this figure display results for $\Delta m/m_0 = \{1, 0.1, 10^{-3}\}$, respectively. The white region appearing in each plot is excluded by the condition $\alpha\delta < -1$. The qualitative results displayed in this figure accord with basic intuition: η is maximized for values of α and δ which come close to saturating the constraint $\alpha\delta < -1$, and smaller values of the ratio $\Delta m/m_0$ for fixed α and δ yield larger values of η. However, the quantitative results displayed in Fig. 2 are less intuitive and quite significant. In particular, we see that $\eta \sim \mathcal{O}(1)$ over a broad range of α and δ values, even in cases in which $\Delta m \sim m_0$. Within this region of parameter space, the full DDM ensemble contributes non-trivially to Ω_{tot}.
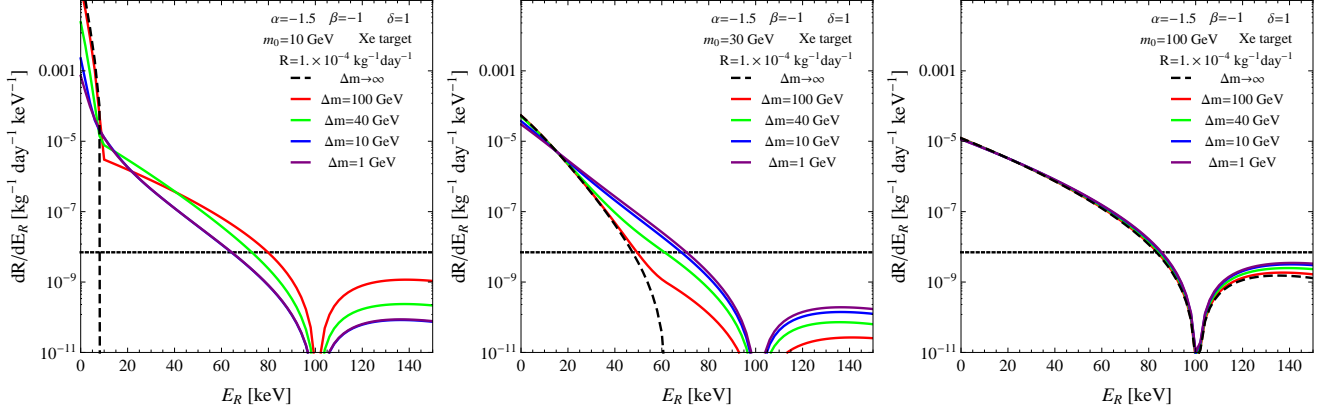

FIG. 3: Recoil-energy spectra associated with DDM ensembles scattering elastically off of a xenon target. In each of the three panels shown, we have set $\alpha = -1.5$, $\beta = -1$, and $\delta = 1$, while the left, center, and right panels correspond to the choices $m_0 = \{10, 30, 100\}$ GeV, respectively. The different curves displayed in each panel correspond to different values of Δm, and each of these curves has been normalized so that the total event rate for nuclear recoils in the energy range $8 \text{ keV} \lesssim E_R \lesssim 48 \text{ keV}$ lies just below the current bound from XENON100 data. Note that the $\Delta m \to \infty$ limit indicated by the dashed black curve corresponds to a traditional dark-matter candidate with a mass $m_\chi = m_0$. The dotted black horizontal line indicates a reasonable estimate of the recoil-energy spectrum for background events at the next generation of liquid-xenon detectors.
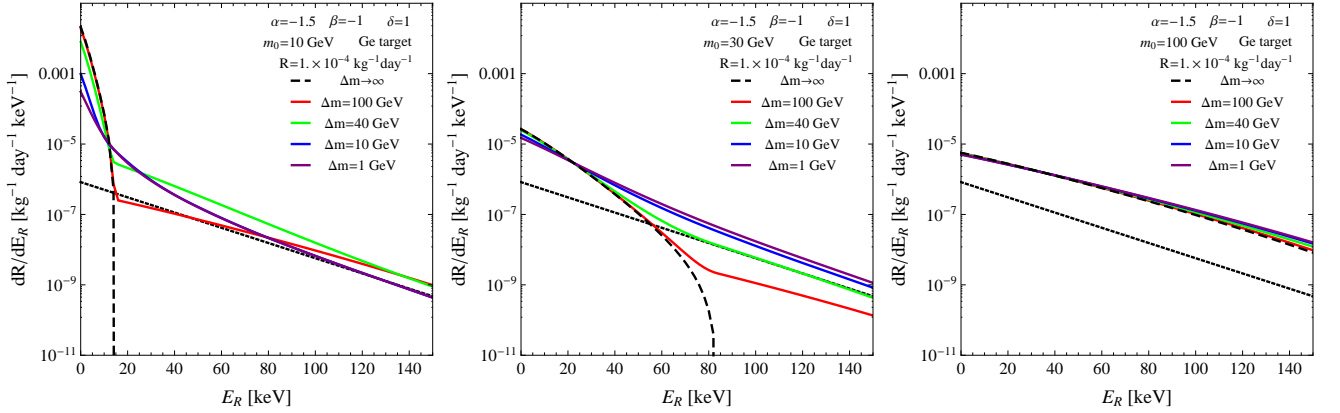

FIG. 4: Recoil-energy spectra associated with DDM ensembles scattering elastically off of a germanium target. The model parameters α, β, and δ have been assigned as in Fig. 3, and we have likewise set $m_0 = \{10, 30, 100\}$ GeV in the left, center, and right panels of the figure, respectively. Each of these curves has been normalized so that the total event rate for nuclear recoils in the energy range $10 \text{ keV} \lesssim E_R \lesssim 100 \text{ keV}$ lies just below the current experimental bound. The dotted black horizontal line indicates a reasonable estimate of the recoil-energy spectrum for background events at the next generation of germanium-crystal detectors.

We now examine the recoil-energy spectra which arise in the context of our simplified DDM model and identify characteristic features in these spectra. A representative set of such spectra is shown for a xenon target in Fig. 3 and for a germanium target in Fig. 4. In each of the three panels shown in each figure, we have set $\alpha = -1.5$, $\beta = -1$, and $\delta = 1$, while the left, center, and right panels in each figure correspond to $m_0 = \{10, 30, 100\}$ GeV, respectively.

These values have been chosen in order to illustrate the different effects to which DDM ensembles can give rise. The different curves displayed in each panel correspond to different values of Δm. Each of the curves displayed in Fig. 3 has been normalized such that the total event rate for nuclear recoils in the energy range $8 \text{ keV} \lesssim E_R \lesssim 48 \text{ keV}$ is $R = 1.0 \times 10^{-4} \text{ kg}^{-1}\text{day}^{-1}$. Likewise, each of the curves displayed in Fig. 4 has been normalized so that this same total event rate is obtained for nuclear recoils in the energy range $10 \text{ keV} \lesssim E_R \lesssim 100 \text{ keV}$. Note that this rate is consistent with current experimental limits on the total event rate for both target materials; moreover, these recoil-energy ranges are chosen to coincide with those typically considered at experiments based on these respective target materials. For reference, we also include a curve (the dotted black horizontal line) in Fig. 3 indicating a reasonable estimate of the recoil-energy spectrum for background events at the next generation of liquid-xenon detectors (to be discussed in more detail in Sect. V). We likewise include an analogous curve in Fig. 4 indicating a reasonable estimate of the background spectrum at the next generation of germanium-crystal detectors.

The results displayed in Figs. 3 and 4 demonstrate that the recoil-energy spectra associated with DDM ensembles and those associated with traditional dark-matter models differ very little for large m_0. This reflects the fact that the shape of the contribution to the recoil-energy spectrum from any individual constituent particle χ_j is not particularly sensitive to m_j for $m_j \gtrsim 40 \text{ GeV}$. Consequently, for $m_0 \gtrsim 40 \text{ GeV}$, the contributions from all of the χ_j in the ensemble manifest roughly the same profile, and the shape of the overall spectrum differs little from that obtained in traditional dark-matter models.

By contrast, the discrepancy between the recoil-energy spectra associated with DDM ensembles and those associated with traditional dark-matter models can be quite striking for small m_0. In particular, two distinctive features emerge which serve to distinguish the recoil-energy spectra associated with DDM ensembles from those associated with traditional dark-matter candidates in this regime. The first of these is an apparent "kink" in the spectrum which arises for $m_0 \lesssim 20 \text{ GeV}$ and large Δm. Physically, this kink occurs because the contribution from χ_0 to the differential event rate dominates at small E_R, but falls sharply as E_R increases. By contrast, the contribution from each of the remaining, heavier χ_j falls far less sharply with recoil energy; hence these contributions collectively dominate at large E_R. The kink represents the transition point between these two E_R regimes. Similar kinks also arise, for example, in the recoil-energy spectra of two-component dark-matter models [8].

The second distinctive feature which appears in the recoil-energy spectra displayed in Figs. 3 and 4 emerges in cases in which m_0 and Δm are both quite small. In this case, a large number of the χ_j are sufficiently light that the profiles of their individual contributions to the differential event rate depend quite sensitively on m_j. Moreover, these individual contributions cannot be resolved for small Δm; rather, they collectively conspire to produce an upturning (indeed, an upward concavity) of the recoil-energy spectrum at low E_R. The characteristic "S"-shaped or "ogee"-shaped curve which results from this upturning is most strikingly manifest in the $\Delta m = \{1, 10\} \text{ GeV}$ curves in the left panel of each figure. This ogee shape is a distinctive feature of DDM ensembles and is difficult to realize in traditional dark-matter models or in multi-component dark matter models involving only a small number of dark-sector fields. As we shall see in Sect. V, both the kink and ogee features highlighted here can serve to distinguish DDM ensembles at future direct-detection experiments.

IV. CONSTRAINING DDM ENSEMBLES WITH CURRENT DIRECT-DETECTION DATA

We begin our analysis of the direct-detection phenomenology of DDM ensembles by assessing how current experimental data constrain the parameter space of our simplified DDM model. The most stringent limit on spin-independent interactions between dark matter and atomic nuclei is currently that established by the XENON100 experiment [19] on the basis of 224.56 live days of observation [20] with a fiducial mass of 34 kg of liquid xenon. Two events were observed within the recoil-energy window $6.6 \text{ keV} \leq E_R \leq 30.6 \text{ keV}$ which passed all cuts, and 1.0 ± 0.2 background events were expected. Under the standard assumptions about the velocity distribution of the particles in the dark-matter halo outlined in Sect. II, *etc.*, this result excludes at 90% C.L. *any* dark-matter candidate — be it a traditional candidate or a DDM ensemble — for which the total rate for nuclear recoils with E_R within this recoil-energy window fails to satisfy the constraint

$$R \lesssim 4.91 \times 10^{-4} \text{ kg}^{-1} \text{ day}^{-1} . \tag{4.1}$$

In any arbitrary DDM model, the total event rate R for nuclear recoils observed at a given detector is obtained by integrating the differential rate in Eq. (3.4) over the range of E_R values which fall within the particular energy window $E_R^{\min} \leq E_R \leq E_R^{\max}$ established for that detector. The contribution to this total rate from each χ_j is also scaled by an acceptance factor $\mathcal{A}_j(E_R)$ which depends both on its mass m_j and on recoil energy. In our simplified

DDM model, we therefore have

$$R = \frac{\sigma_{n0}^{(\mathrm{SI})}\rho_{\mathrm{tot}}^{\mathrm{loc}}A^2}{2\mu_{n0}^2 m_0}(1-\eta)\int_{E_R^{\mathrm{min}}}^{E_R^{\mathrm{max}}}dE_R F^2(E_R)\sum_{j=0}^{\infty}\mathcal{A}_j(E_R)I_j(E_R)\left(1+j^\delta\frac{\Delta m}{m_0}\right)^{\alpha+2\beta-1}. \tag{4.2}$$

In practice, the dependence of $\mathcal{A}_j(E_R)$ on both E_R and m_j tends to be slight over the range of E_R values typically considered in noble-liquid and solid-state detectors. We therefore approximate $\mathcal{A}_j(E_R)\approx 0.5$ for all χ_j in our analysis of the XENON100 constraint, in accord with the acceptance values quoted in Ref. [19].

In Fig. 5, we display a series of contour plots showing the 90% C.L. limit in Eq. (4.1) expressed as a bound on $\sigma_{n0}^{(\mathrm{SI})}$ in our simplified DDM model. Of course, for large Δm, the 90% C.L. limit value of $\sigma_{n0}^{(\mathrm{SI})}$ approaches the limit [20] on $\sigma_{n\chi}^{(\mathrm{SI})}$ for a traditional dark-matter candidate with mass $m_\chi \approx m_0$. However, when Δm is small and a larger number of states contribute significantly to the total event rate, the experimental limit can differ substantially from that obtained for a traditional dark-matter candidate. Such deviations become particularly pronounced for $m_0 \lesssim 10$ GeV, in which case the majority of nuclear-recoil events initiated by the lightest constituent χ_0 in the ensemble have E_R values which lie below the detector threshold. In this region, the heavier χ_j collectively provide the dominant contribution to the total event rate. However, it is evident from Fig. 5 that the heavier χ_j can also play an important role in the direct-detection phenomenology of DDM models even in the regime in which $m_0 \gtrsim 10$ GeV.

V. DISTINGUISHING DDM ENSEMBLES AT FUTURE DETECTORS

We now examine the potential for distinguishing DDM ensembles from traditional dark-matter candidates at future direct-detection experiments. Of course, an initial discovery of either a DDM ensemble or a traditional dark-matter candidate at a given direct-detection experiment would take the form of an excess in the total number of nuclear-recoil events observed above the expected background. Our principal aim is therefore to determine the degree to which replacing the traditional dark-matter candidate with a DDM ensemble — keeping all other aspects of our standard benchmark unchanged — would result in a discernible deviation in the recoil-energy spectra measured at such experiments, once such an excess is observed. For concreteness, we consider the situation in which the total scattering rate lies just below the sensitivity of current experiments, so that a sizable number of signal events is observed.

Our procedure for comparing the recoil-energy spectrum associated with a given DDM ensemble to the spectrum associated with a traditional dark matter candidate with mass m_χ is analogous to that used in Ref. [4] to compare invariant-mass distributions at the LHC in the corresponding theories. Similar procedures were also used in Ref. [8]. In particular, we partition each of the two spectra into n_b bins with widths greater than or equal to the recoil-energy resolution ΔE_R at the minimum E_R in the bin. We then construct the χ^2 statistic

$$\chi^2(m_\chi) = \sum_k \frac{[X_k - \mathcal{E}_k(m_\chi)]^2}{\sigma_k^2}, \tag{5.1}$$

where the index k labels the bin, X_k is the expected population of events in bin k in the DDM model, $\mathcal{E}_k(m_\chi)$ is the expected population of events in bin k in the traditional dark-matter model, and σ_k^2 is the variance in X_k due to statistical uncertainties. Since the X_k are distributed according to a multinomial distribution, it follows that $\sigma_k^2 = X_k(1 - X_k/N_e)$, where N_e denotes the total number of signal events observed.

The proper measure of the distinctiveness of the recoil-energy spectrum associated with a DDM ensemble is not the degree to which it differs from that associated with a traditional dark-matter candidate with a particular m_χ, but rather from *any* such dark-matter candidate. Consequently, we survey over traditional dark-matter candidates χ with different values of m_χ with all other assumptions held fixed. Note that the total event rate R — and hence also the spin-independent cross-section per nucleon $\sigma_{n\chi}^{(\mathrm{SI})}$ for each value m_χ — is effectively specified by the signal-event count N_e; thus m_χ is the only remaining parameter over which we must survey. We then take

$$\chi_{\mathrm{min}}^2 \equiv \min_{m_\chi}\left\{\chi^2(m_\chi)\right\} \tag{5.2}$$

as our measure of the distinctiveness of the recoil-energy spectrum associated with a given DDM ensemble. We then evaluate a statistical significance of differentiation in each case by comparing χ_{min}^2 to a χ^2 distribution with $n_b - 1$ degrees of freedom. Specifically, this is defined to be the significance to which the p-value obtained from this comparison would correspond for a Gaussian distribution.
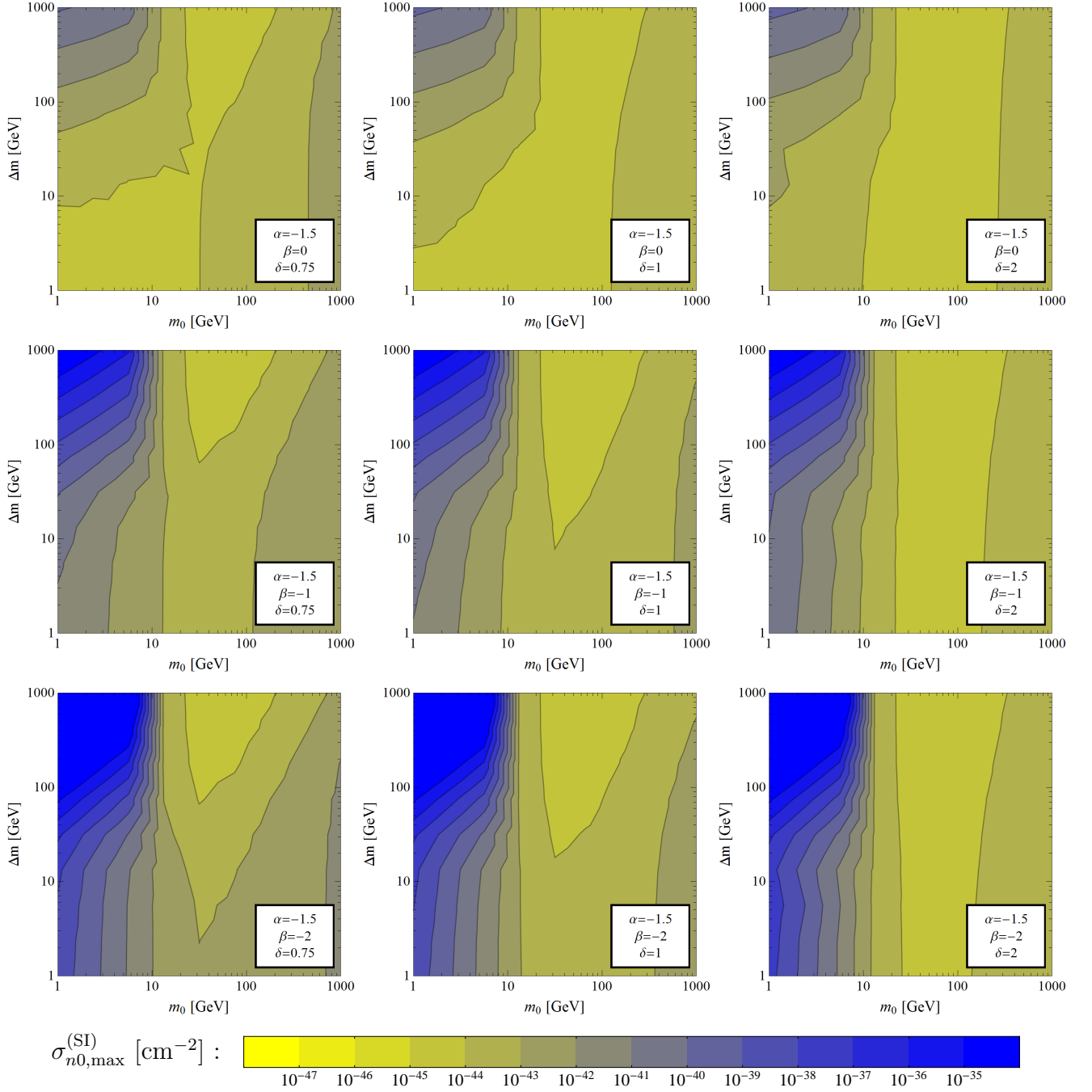
FIG. 5: Contour plots showing the 90% C.L. limit from XENON100 on the spin-independent cross-section per nucleon $\sigma_{n0}^{(SI)}$ (in cm^{-2}) of the lightest constituent particle χ_0 in our simplified DDM model. The panels appearing in the top, center, and bottom rows show results for $\beta = \{0, -1, -2\}$, respectively. The panels appearing in the left, center, and right columns show the results for $\delta = 0.75, 1, 2$, respectively. In each panel, we have set $\alpha = -1.5$.

For this study, we choose not to limit our attention any particular experiment, either existing or proposed; rather, we investigate the prospects for distinguishing DDM ensembles at a pair of hypothetical detectors, each with characteristics representative of a particular class of next-generation direct-detection experiments. The first of these is a dual-phase liquid-xenon detector with attributes similar to those projected for XENON1T and future phases of the LUX experiment. The other is a germanium-crystal detector with attributes similar to those projected for GEODM and the SNOLAB phase of the SuperCDMS experiment. For both experiments, we assume five live years of data

collection time.

Each of these hypothetical detectors is characterized by its recoil-energy resolution ΔE_R, recoil-energy window, signal acceptance, fiducial mass, and the differential event rate associated with the combined background. For our hypothetical next-generation xenon detector, we choose a recoil-energy window $8 \text{ keV} \leq E_R \leq 48 \text{ keV}$, a fiducial mass of 5000 kg, and a signal acceptance $\mathcal{A}_j(E_R) \approx 0.5$ which is independent of both E_R and m_j. We model the energy resolution ΔE_R of our detector after that obtained for the combined S1 and S2 signals at the XENON100 experiment. This energy resolution is determined from measurements of the detector response for a number of γ-ray calibration lines at various energies. The result, expressed in terms of electron-recoil-equivalent energy units keV_{ee}, is [21]

$$\Delta E_R \approx 0.60 \times \left(\frac{E_R}{\text{keV}_{\text{ee}}} \right)^{1/2} \text{keV}_{\text{ee}} . \tag{5.3}$$

The corresponding energy resolution for nuclear recoils is related to this result by an energy-dependent effective quenching factor

$$Q_{\text{eff}}(E_R) \equiv \frac{1}{\mathcal{L}_{\text{eff}}(E_R)} \left(\frac{S_{\text{ee}}}{S_{\text{nr}}} \right) , \tag{5.4}$$

where $\mathcal{L}_{\text{eff}} \equiv L_{\text{nr}}^{(0)} / L_{\text{ee}}^{(0)}$ is the ratio of the light yield for nuclear recoils to that for electron recoils at zero applied electric field, and where $S_{\text{ee}} = 0.58$ and $S_{\text{nr}} = 0.95$ are electric-field-scintillation quenching factors which account for the effect of the 530 V/cm applied drift field [22]. The energy resolution ΔE_R for nuclear recoils therefore depends on the uncertainties in $\mathcal{L}_{\text{eff}}$, S_{ee}, and S_{nr}. For $E_R \gtrsim 3 \text{ keV}$, the uncertainty in $\mathcal{L}_{\text{eff}}$ is approximately independent of E_R and given by $\Delta \mathcal{L}_{\text{eff}} \approx 0.01$, while the uncertainty in S_{ee} and S_{nr} is negligible. We therefore find that over the full recoil-energy window of our hypothetical detector, ΔE_R is given by

$$\Delta E_R \approx \left[0.36 \left(\frac{E_R}{\text{keV}} \right) + \left(\frac{0.01}{\mathcal{L}_{\text{eff}}(E_R)} \right)^2 \left(\frac{E_R}{\text{keV}} \right)^2 \right]^{1/2} \text{keV} , \tag{5.5}$$

where all energies are expressed in nuclear-recoil-equivalent units.

We model the differential event rate for the combined background at our hypothetical xenon detector after that projected for the combined background at XENON1T. This background rate, after the application of event-selection criteria (including both a multiple-scatter veto and an S2/S1 cut), is dominated by electron-recoil events, and in particular those from ^{85}Kr and other impurities within the detector volume. The recoil-energy spectrum associated with this background is approximately independent of E_R, and for a ^{85}Kr concentration of 0.5 ppt is given by [23]

$$\left(\frac{dR}{dE_R} \right)_{\text{BG}} \approx 7 \times 10^{-9} \text{ kg}^{-1} \text{day}^{-1} \text{keV}^{-1} . \tag{5.6}$$

For our hypothetical next-generation germanium detector, we likewise choose the fiducial mass to be 5000 kg. Moreover, we choose a recoil-energy acceptance window, energy resolution, and signal acceptance comparable with that of the CDMS II experiment. The recoil-energy acceptance window for CDMS II is $10 \text{ keV} \leq E_R \leq 100 \text{ keV}$, and the energy resolution ΔE_R within this range is given by [24]

$$\Delta E_R \approx 0.2 \times \left(\frac{E_R}{\text{keV}} \right)^{1/2} \text{keV} . \tag{5.7}$$

We adopt this same acceptance window and energy resolution for our hypothetical next-generation detector. The signal acceptance for CDMS II varies only slightly, from a minimum of $\mathcal{A} \approx 0.25$ at E_R values near the endpoints $E_R^{\min} = 10 \text{ keV}$ and $E_R^{\max} = 100 \text{ keV}$ of the recoil-energy acceptance window to a maximum of $\mathcal{A} \approx 0.32$ at $E_R \sim 20 \text{ keV}$ [25, 26]. We therefore once again approximate the acceptance as independent of E_R and m_j, and take $\mathcal{A}_j = 0.3$ for all χ_j for our hypothetical detector.

In order to obtain a realistic recoil-energy spectrum for the combined background at our hypothetical germanium detector, we adopt the following procedure. We model the shape of this spectrum after that observed for the CDMS II experiment, which is dominated at $E_R \gtrsim 10 \text{ keV}$ by the contribution from surface events, and adopt a normalization such that the total event rate is $R_{\text{BG}} \approx 1.0 \times 10^{-5} \text{ kg}^{-1} \text{ day}^{-1}$. This is a rate comparable to the background-event rate estimates for the SuperCDMS detector at SNOLAB. At recoil energies $E_R \gtrsim 10 \text{ keV}$, the background rate at the CDMS II detector is dominated by the contribution from surface events. For $10 \text{ keV} \lesssim E_R \lesssim 25 \text{ keV}$, the recoil-energy spectrum is well modeled by [27]

$$\left(\frac{dR}{dE_R} \right) \approx \left(8.3 \times 10^{-7} \right) \times e^{-0.05 \times (E_R/\text{keV})} \text{ kg}^{-1} \text{day}^{-1} \text{keV}^{-1} . \tag{5.8}$$

From this result, we extrapolate the background spectrum over the full recoil-energy window of our detector.

We consider the situation in which the total rate for nuclear-recoil events engendered by the DDM ensemble lies just below the sensitivity of current experiments, in which case the number of signal events observed at the next generation of detectors will be substantial. We examine the DDM differentiation prospects at each of our hypothetical detectors independently, in isolation, rather than attempting to correlate the results between the two. For concreteness, we adopt a benchmark value of $N_e = 1000$ total signal events at each detector. Note that for our chosen running time of five live years, this value of N_e is consistent with the XENON100 limits discussed in Sect. IV throughout the entirety of the parameter space of our simplified DDM model which we include in our analysis for both of our detectors.

In Fig. 6 we show how the projected statistical significance of differentiation obtained with $N_e = 1000$ signal events at our hypothetical xenon detector varies as a function of the parameters which characterize our simplified DDM model. We find that from among these parameters, the significance is particularly sensitive to the values of m_0 and Δm; hence we display our results in $(m_0, \Delta m)$ space, with α, β, and δ held fixed in each of the panels shown. The panels in the left, center, and right columns of the figure correspond respectively to $\delta = \{0.75, 1, 2\}$, and the panels in the top, center, and bottom rows correspond to $\beta = \{-2, -1, 0\}$. In all of the panels shown, we have set $\alpha = -1.5$.

The results displayed in Fig. 6 are fundamentally due to the interplay between the individual dR/dE_R contributions from two different classes of χ_j within a given ensemble: those in with masses $m_j \lesssim 20$ GeV (the "low-mass dark matter" regime) and those with $m_j \gtrsim 20$ GeV (the "high-mass dark matter" regime). As illustrated in Fig. 1, contributions to the recoil-energy spectrum from the χ_j in the low-mass regime begin to fall precipitously within or below the recoil-energy window for our hypothetical detector. Moreover, the value of E_R at which this drop-off occurs is quite sensitive to m_j for χ_j in this regime. By contrast, this suppression effect only becomes manifest for the χ_j in the high-mass regime at E_R values far beyond the recoil-energy-acceptance window of our detector. The spectra fall far more gradually with E_R for these fields, and their overall shape depends far less sensitively on m_j.

This distinction between these two mass regimes plays a critical role in determining the significance with which one can distinguish DDM ensembles from traditional dark-matter candidates at direct-detection experiments. For example, it implies that any DDM ensemble in which all of the constituents in the ensemble fall within the high-mass regime is generically difficult to distinguish from traditional dark-matter candidates which likewise fall in the high-mass regime. Indeed, we see in Fig. 6 that it is quite difficult to distinguish a DDM ensemble in situations in which $m_0 \gtrsim 20$ GeV, irrespective of the values of β and δ. A similar behavior is also manifest in the region of parameter space within which $m_0 \lesssim 5$ GeV and $\Delta m \gtrsim 20$ GeV, again regardless of β and δ. This arises because the vast majority of nuclear recoils initiated by any χ_j with $m_j \lesssim 5$ GeV have E_R values which fall below the detector threshold $E_R^{\min}$. The contribution to the total recoil-energy spectrum for any χ_j with m_j in this region is therefore essentially invisible. Consequently, in cases in which $m_0 \lesssim 5$ GeV while $\Delta m \gtrsim 20$ GeV, only the contributions from the χ_j in the high-mass regime are evident and the distinguishing power is once again low.

By contrast, within other substantial regions of the parameter space of our simplified DDM model, the statistical significance of differentiation is quite high. For example, in each panel displayed in Fig. 6, there exists a particular range of Δm values within which a 5σ significance is obtained for $5 \lesssim m_0 \lesssim 20$ GeV. Within this region, the kink behavior evinced in several of the recoil-energy spectra displayed in Fig. 3 can be distinguished. The range of Δm values within which this is possible depends primarily on the value of β. When β is small and the coupling to the heavier χ_j is suppressed, the prospects for distinguishing a DDM ensemble on the basis of this feature becomes significant when Δm is such that the mass of the next-to-lightest constituent χ_1 lies just above the threshold $m_1 \sim 20$ GeV of the high-mass regime. These prospects remain high until Δm reaches the point at which the collective contribution to the recoil-energy spectrum from the χ_j in the high-mass regime falls below the sensitivity of the detector. As β increases, this contribution remains substantial for larger and larger Δm. However, increasing β also results in this contribution becoming sufficiently large for small Δm that it overwhelms the contribution from χ_0 and yields an overall spectrum indistinguishable from that of a traditional dark-matter candidate with m_χ in the high-mass regime. The consequences of these two effects are apparent in Fig. 6, which shows how the region of elevated significance due to the resolution of a kink in the recoil-energy spectrum shifts from 10 GeV $\lesssim \Delta m \lesssim 50$ GeV for $\beta = -2$ to 70 GeV $\lesssim \Delta m \lesssim 800$ GeV for $\beta = 0$.

Another region of parameter space within which kinks in the recoil-energy spectrum frequently lead to an enhancement in the significance of differentiation is that within which $m_0 \lesssim 5$ GeV and 7 GeV $\lesssim \Delta m \lesssim 20$ GeV. Indeed, such an enhancement is evident in many of the panels in Fig. 6. Within this region, m_0 is sufficiently light that the contribution from χ_0 to the recoil-energy spectrum is hidden beneath the detector threshold, m_1 lies within the low-mass region, and all of the remaining m_j with $j \geq 2$ lie within the high-mass regime. Thus, within this region, χ_1 plays the same role which χ_0 plays in the region of parameter space discussed above.

In a number of the panels displayed in Fig. 6 — and especially those in which $\delta \lesssim 1$ — we obtain a sizeable significance of differentiation for our DDM ensemble not merely within this region, but over a substantial region of the parameter space within which $m_0, \Delta_m \lesssim 20$ GeV. Indeed, throughout much of this region, there exist multiple χ_j with closely-spaced m_j in the low-mass regime. When this is the case, the corresponding recoil-energy spectrum for the
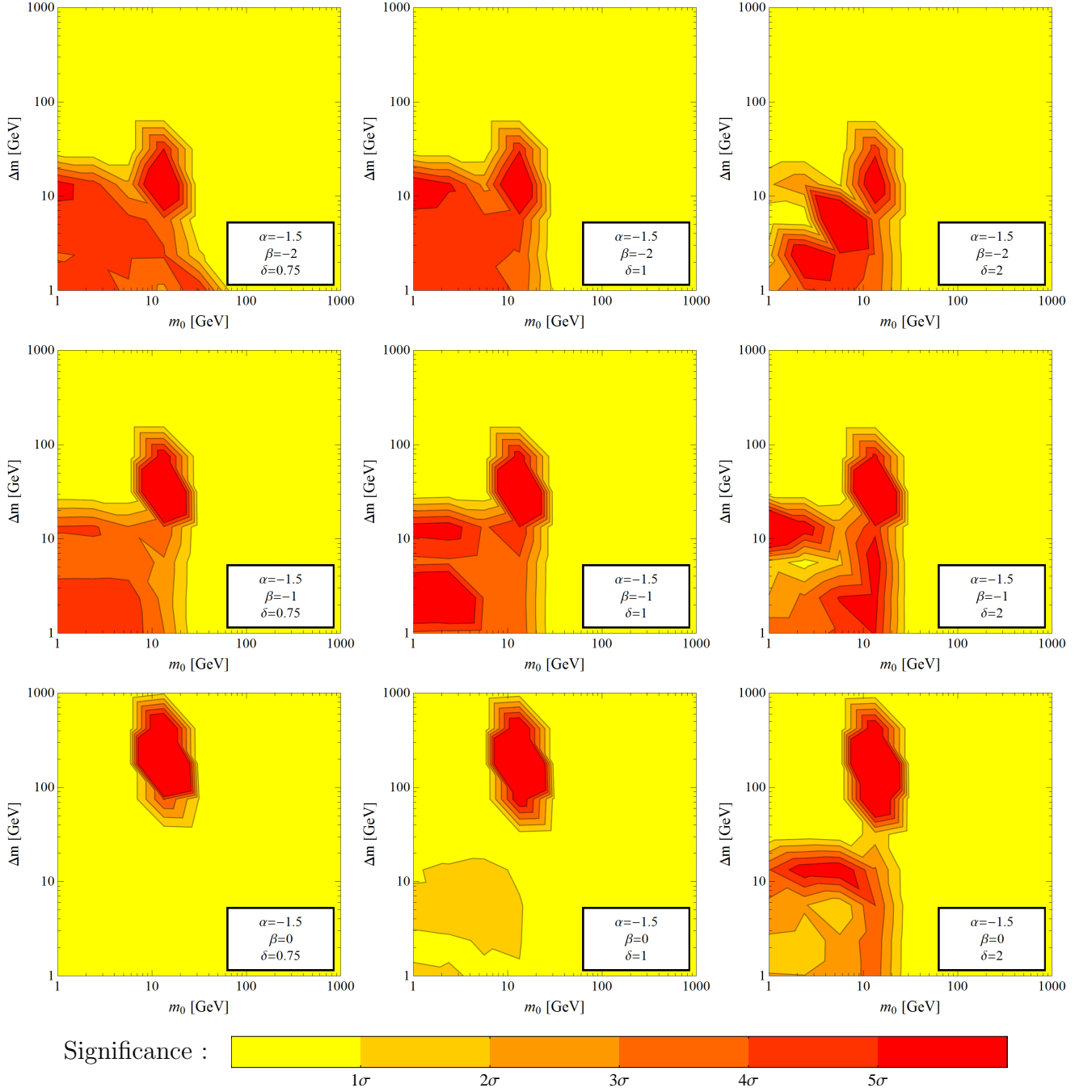
FIG. 6: Contour plots showing the significance level at which the recoil-energy spectrum associated with a DDM ensemble can be distinguished from that associated with *any* traditional dark-matter candidate which gives rise to the same total event rate at a hypothetical direct-detection experiment. This experiment is taken to be a liquid-xenon detector with a fiducial volume of 5000 kg and characteristics otherwise similar to those of the proposed XENON1T experiment, as discussed in the text. A running time of five live years and an event count of $N_e = 1000$ signal events is assumed.

DDM ensemble assumes the characteristic ogee shape discussed in Sect. III. This ogee shape is a distinctive feature of DDM scenarios with small Δm, and serves as an effective discriminant between such scenarios and traditional dark-matter models.

As is evident from the results shown in Fig. 6, the significance of differentiation depends on δ in a somewhat complicated manner. Broadly speaking, the significance of differentiation obtained for $m_0, \Delta m \lesssim 20$ GeV tends to

decrease as δ decreases, especially for large β. The primary reason for this is that the density of states in the ensemble increases rapidly with m_j when δ is small, and thus a greater proportion of Ω_{tot} is carried by the χ_j in the high-mass regime. Provided that β is sufficiently large that a sizeable number of these χ_j couple to nucleons with reasonable strength, their collective contribution to the differential event rate tends to overwhelm that of the χ_j in the low-mass regime. Moreover, even when the low-mass constituents do contribute significantly to the overall rate, the curvature of the ogee shape becomes less pronounced — and therefore more difficult to distinguish — as β increases. By contrast, when δ is large, the lighter χ_j carry a greater proportion of Ω_{tot}, and their contributions to the recoil-energy spectrum are more readily resolved. However, increasing δ also increases the mass splittings among the lighter χ_j. This has the dual effect of pushing a greater and greater number of the χ_j into the high-mass regime and making the individual contributions of the remaining constituents in the low-mass region easier to resolve. As a result, the broad regions of parameter space throughout which a DDM ensemble could be distinguished on the basis of a characteristic ogee feature in the recoil-energy spectrum for small δ are replaced at large δ by a set of "islands" in which a kink in the spectrum is the distinguishing feature. These effects are already apparent in the right column of Fig. 6.
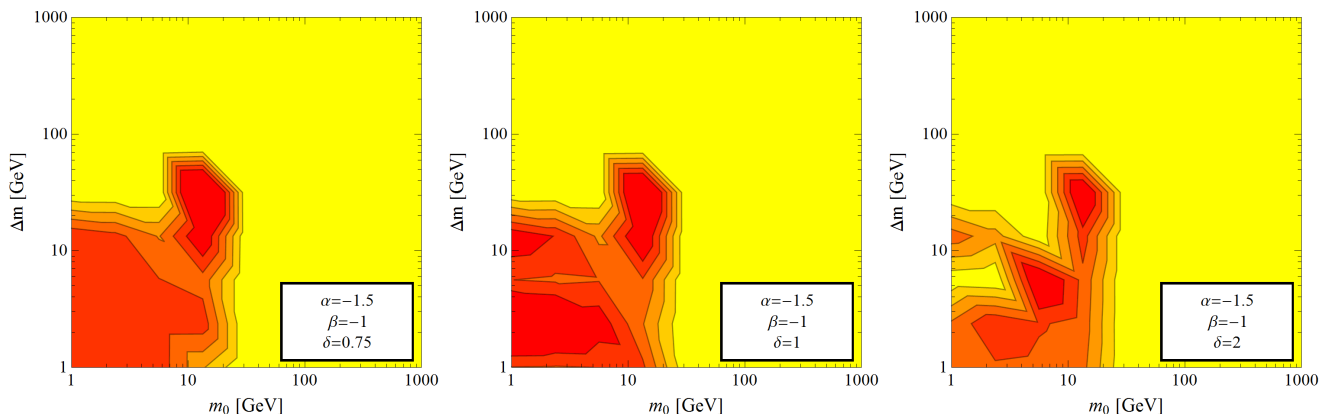

FIG. 7: Contour plots showing the significance level at which the recoil-energy spectrum associated with a DDM ensemble can be distinguished from that associated with *any* traditional dark-matter candidate which gives rise to the same total event rate at a hypothetical germanium-crystal detector. The colored regions shown correspond to the same significance intervals as in Fig. 3. The detector is taken to have a fiducial volume of 5000 kg and characteristics otherwise similar to those of the proposed SNOLAB phase of the SuperCDMS experiment, as discussed in the text. Once again, running time of five live years and an event count of $N_e = 1000$ signal events is assumed.

Let us now compare these results to the results we obtain for our hypothetical germanium-crystal detector. In Fig. 7, we show the projected statistical significance of differentiation obtained with $N_e = 1000$ signal events at this hypothetical detector. The panels in the left, center, and right columns of the figure correspond respectively to $\delta = \{0.75, 1, 2\}$, and in each of these three panels we have set $\alpha = -1.5$ and $\beta = -1$. It is evident from Fig. 7 that while the quantitative results obtained for our two hypothetical detectors differ due to differences in the mass of the target nucleus, the observed spectrum of background events, *etc.*, the qualitative results are quite similar. For $5 \text{ GeV} \lesssim m_0 \lesssim 20 \text{ GeV}$, there exists a range of Δm values within which the presence of a discernible kink in the recoil-energy spectrum leads to a 5σ significance of differentiation. In addition, a similarly high significance is obtained for $\Delta m, m_0 \lesssim 20 \text{ GeV}$ due either to the similar kink features (at large δ) or to the characteristic ogee shape to which DDM ensembles can give rise when mass splittings are small (at small δ).

VI. DISCUSSION AND CONCLUSIONS

In this paper, we have investigated the potential for discovering a DDM ensemble and differentiating it from a traditional dark-matter candidate at the next generation of dark-matter direct-detection experiments. In particular, we have assessed the degree to which these two classes of dark-matter candidates may be distinguished on the basis of differences in recoil-energy spectra. We have demonstrated that DDM ensembles give rise to a number of characteristic features in such spectra, including observable kinks and distinctive ogee profiles. Moreover, we have demonstrated that under standard assumptions, the identification of such features can serve to distinguish a DDM ensemble from any traditional dark-matter candidate at the 5σ significance level at the next generation of direct-detection experiments. We have found that the prospects for differentiation are particularly auspicious in cases in which the mass splittings

between the constituent fields in the DDM ensemble are small and in which the mass of the lightest such field is also relatively small. Note that this is also a regime in which a large fraction of the full DDM ensemble contributes meaningfully to Ω_{CDM}.

It is also interesting to compare the prospects for distinguishing DDM ensembles at direct-detection experiments to the prospects for distinguishing them at the LHC. We have demonstrated here that the former are greatest when $m_0 \lesssim 20$ GeV, Δm is small, $0.25 \lesssim \delta \lesssim 2$, and the effective couplings between the χ_j and SM particles decrease moderately with m_j. By contrast, it was shown in Ref. [4] that the latter are greatest when Δm is small, $\delta \lesssim 1$, and the effective couplings to SM particles increase with m_j. Thus, we see that these two experimental methods of distinguishing DDM ensembles are effective in somewhat different regions of parameter space, and are therefore complementary. However, we note that there is one region in which evidence for a DDM ensemble may manifest itself both at direct-detection experiments and at the LHC. This is the region in which $m_0 \lesssim 20$ GeV, $0.25 \lesssim \delta \lesssim 0.75$, the effective couplings to SM particles are roughly independent of mass, and Δm is also either quite small or else within the range in which an observable kink arises in the recoil-energy spectrum. The simultaneous observation of both collider and direct-detection signatures in this case would provide highly compelling experimental evidence for a DDM ensemble.

Needless to say, there are numerous additional directions potentially relevant for direct detection which we have not explored in this paper. For example, we have not considered the prospects for distinguishing DDM ensembles at argon- or carbon-based detectors, or instruments involving target materials other than xenon and germanium. Likewise, we have not considered the prospects for observing an annual modulation in the signal rate at direct-detection experiments — a strategy long employed by the DAMA experiment and more recently by CoGeNT. We have also not considered directional detection. More generally, We have not considered modifications of the astrophysical assumptions (such as the halo-velocity distributions) or nuclear-form-factor model which define our standard benchmark. Finally, we have not endeavored to compare or correlate signals from multiple detectors using different target materials. These directions are all ripe for further study [28].

In a similar vein, in this paper we have restricted our attention to cases in which elastic processes dominate the scattering rate for all particles in the DDM ensemble. However, within the context of the DDM framework, inelastic scattering processes [29–31] of the form $\chi_j N \to \chi_k N$ where $j \neq k$ also occur, and can contribute significantly to this rate when $\Delta m \lesssim \mathcal{O}(100 \text{ keV})$. This possibility is particularly interesting for a number of reasons. For example, in DDM scenarios, the final-state particle in such inelastic scattering events can be a heavier particle in the ensemble, as in typical inelastic dark-matter models, but it can also be a *lighter* particle in the ensemble. In other words, inelastic scattering in the DDM framework involves both "upscattering" and "downscattering" processes. This latter possibility is a unique feature of DDM scenarios, given that the initial-state particle χ_j need not be the lightest particle in the dark sector. Moreover, as we have demonstrated above, the range of Δm relevant for inelastic scattering is also one in which the characteristic features to which DDM ensembles give rise are particularly pronounced.

Some of the consequences of such inelastic processes are readily apparent. For example, let us consider the case in which $|\delta m_{jk}| \ll m_j, m_k$, where $\delta m_{jk} \equiv m_k - m_j$. Although the matrix element for inelastic scattering is, to leading order, of the same form as for an elastic interaction, the kinematics can be very different. In the limit $|\delta m_{jk}| \ll m_j, m_k$, the maximum recoil energy E_{jk}^+ and minimum recoil energy E_{jk}^- possible in inelastic scattering are given by

$$E_{jk}^{\pm} = \frac{2\mu_{Nj}^2 v^2}{m_N} \left(1 - \frac{\delta m_{jk}}{\mu_{Nj} v^2} \pm \sqrt{1 - 2\frac{\delta m_{jk}}{\mu_{Nj} v^2}} \right) \tag{6.1}$$

where v is the relative velocity of the initial particles. If $\delta m_{jk} > 0$, then this upscattering process is similar to that typically considered in models of inelastic dark matter [29, 30], and its basic effect is to narrow the range of recoil energies for which scattering is possible for a fixed dark-matter velocity relative to the Earth. A general result of this effect is that heavier components of the DDM ensemble are "brought into range" of a direct-detection experiment, which can then resolve the recoil-energy endpoint. For $\delta m_{jk} < 0$, however, the range of possible recoil energies is broadened. As a result, low-mass members of the DDM ensemble can produce recoils which lie above the recoil-energy threshold $E_R^{\min}$ of a particular experiment. Moreover, we note that the matrix element for the process $\chi_j N \to \chi_k N$ determines the matrix element for the process $\chi_k N \to \chi_j N$ through crossing symmetry. For a DDM ensemble with a fixed distribution of densities, the scattering rates of different components can thus be related to each other. All of these possibilities will be discussed further in Ref. [32].

[1] K. R. Dienes and B. Thomas, Phys. Rev. D **85**, 083523 (2012) [arXiv:1106.4546 [hep-ph]].
[2] K. R. Dienes and B. Thomas, Phys. Rev. D **85**, 083524 (2012) [arXiv:1107.0721 [hep-ph]].
[3] K. R. Dienes and B. Thomas, arXiv:1203.1923 [hep-ph], to appear in Phys. Rev. D.
[4] K. R. Dienes, S. Su and B. Thomas, arXiv:1204.4183 [hep-ph], to appear in Phys. Rev. D.
[5] M. W. Goodman and E. Witten, Phys. Rev. D **31**, 3059 (1985).
[6] For reviews, see, *e.g.*:
    G. Jungman, M. Kamionkowski and K. Griest, Phys. Rept. **267**, 195 (1996) [arXiv:hep-ph/9506380];
    D. Hooper, [arXiv:0901.4090 [hep-ph]];
    N. Weiner, "Dark Matter Theory," video lectures given at TASI 2009,
    http://physicslearning2.colorado.edu/tasi/tasi_2009/tasi_2009.htm;
    J. L. Feng, Ann. Rev. Astron. Astrophys. **48**, 495 (2010) [arXiv:1003.0904 [astro-ph.CO]];
    R. W. Schnee, arXiv:1101.5205 [astro-ph.CO].
[7] For example, see:
    T. Hur, H. S. Lee and S. Nasri, Phys. Rev. D **77**, 015008 (2008) [arXiv:0710.2653 [hep-ph]];
    J. L. Feng and J. Kumar, Phys. Rev. Lett. **101**, 231301 (2008) [arXiv:0803.4196 [hep-ph]];
    H. Sung Cheon, S. K. Kang and C. S. Kim, Phys. Lett. B **675**, 203 (2009) [arXiv:0807.0981 [hep-ph]];
    K. M. Zurek, Phys. Rev. D **79**, 115002 (2009) [arXiv:0811.4429 [hep-ph]];
    B. Batell, M. Pospelov and A. Ritz, Phys. Rev. D **79**, 115019 (2009) [arXiv:0903.3396 [hep-ph]];
    F. Chen, J. M. Cline and A. R. Frey, Phys. Rev. D **80**, 083516 (2009) [arXiv:0907.4746 [hep-ph]];
    I. Cholis and N. Weiner, arXiv:0911.4954 [astro-ph.HE];
    X. Gao, Z. Kang and T. Li, Eur. Phys. J. C **69**, 467 (2010) [arXiv:1001.3278 [hep-ph]];
    D. Feldman, Z. Liu, P. Nath and G. Peim, Phys. Rev. D **81**, 095017 (2010) [arXiv:1004.0649 [hep-ph]];
    P. T. Winslow, K. Sigurdson and J. N. Ng, Phys. Rev. D **82**, 023512 (2010) [arXiv:1005.3013 [hep-ph]];
    J. L. Feng, M. Kaplinghat and H. -B. Yu, Phys. Rev. D **82**, 083525 (2010) [arXiv:1005.4678 [hep-ph]];
    M. Aoki, M. Duerr, J. Kubo and H. Takano, arXiv:1207.3318 [hep-ph].
[8] S. Profumo, K. Sigurdson and L. Ubaldi, JCAP **0912**, 016 (2009) [arXiv:0907.4374 [hep-ph]].
[9] J. D. Lewin and P. F. Smith, Astropart. Phys. **6**, 87 (1996).
[10] C. Savage, G. Gelmini, P. Gondolo and K. Freese, JCAP **0904**, 010 (2009) [arXiv:0808.3607 [astro-ph]].
[11] M. C. Smith *et al.*, Mon. Not. Roy. Astron. Soc. **379**, 755 (2007) [arXiv:astro-ph/0611671].
[12] R. H. Helm, Phys. Rev. **104**, 1466 (1956);
     J. Engel, Phys. Lett. B **264**, 114 (1991).
[13] J. L. Feng, J. Kumar, D. Marfatia and D. Sanford, Phys. Lett. B **703**, 124 (2011) [arXiv:1102.4331 [hep-ph]].
[14] S. Chang, N. Weiner and I. Yavin, Phys. Rev. D **82**, 125011 (2010) [arXiv:1007.4200 [hep-ph]];
     V. Barger, W. -Y. Keung and D. Marfatia, Phys. Lett. B **696**, 74 (2011) [arXiv:1007.4345 [hep-ph]].
[15] For example, see:
     A. Gould, Astrophys. J. **368**, 610 (1991);
     D. Stiff, L. M. Widrow and J. Frieman, Phys. Rev. D **64**, 083516 (2001) [astro-ph/0106048];
     K. Freese, P. Gondolo, H. J. Newberg and M. Lewis, Phys. Rev. Lett. **92**, 111301 (2004) [astro-ph/0310334];
     J. Lundberg and J. Edsjo, Phys. Rev. D **69**, 123505 (2004) [astro-ph/0401113];
     C. Savage, K. Freese and P. Gondolo, Phys. Rev. D **74**, 043531 (2006) [astro-ph/0607121];
     M. Fairbairn and T. Schwetz, JCAP **0901**, 037 (2009) [arXiv:0808.0704 [hep-ph]];
     J. March-Russell, C. McCabe and M. McCullough, JHEP **0905**, 071 (2009) [arXiv:0812.1931 [astro-ph]];
     A. H. G. Peter, Phys. Rev. D **79**, 103531 (2009) [arXiv:0902.1344 [astro-ph.HE]]; Phys. Rev. D **79**, 103533 (2009) [arXiv:0902.1348 [astro-ph.HE]];
     F. -S. Ling, Phys. Rev. D **82**, 023534 (2010) [arXiv:0911.2321 [astro-ph.GA]];
     M. Kuhlen, N. Weiner, J. Diemand, P. Madau, B. Moore, D. Potter, J. Stadel and M. Zemp, JCAP **1002**, 030 (2010) [arXiv:0912.2358 [astro-ph.GA]];
     R. F. Lang and N. Weiner, JCAP **1006**, 032 (2010) [arXiv:1003.3664 [hep-ph]];
     J. Edsjo and A. H. G. Peter, arXiv:1004.5258 [astro-ph.EP];
     C. McCabe, Phys. Rev. D **82**, 023530 (2010) [arXiv:1005.0579 [hep-ph]];
     A. Natarajan, Adv. Astron. **2011**, 285346 (2011) [arXiv:1006.5716 [astro-ph.CO]];
     A. M. Green, JCAP **1010**, 034 (2010) [arXiv:1009.0916 [astro-ph.CO]]; Mod. Phys. Lett. A **27**, 1230004 (2012) [arXiv:1112.0524 [astro-ph.CO]];
     P. J. Fox, G. D. Kribs and T. M. P. Tait, Phys. Rev. D **83**, 034007 (2011) [arXiv:1011.1910 [hep-ph]];

      M. T. Frandsen, F. Kahlhoefer, C. McCabe, S. Sarkar and K. Schmidt-Hoberg, JCAP **1201**, 024 (2012) [arXiv:1111.0292 [hep-ph]].

[16] P. Salucci, F. Nesti, G. Gentile and C. F. Martins, Astron. Astrophys. **523**, A83 (2010) [arXiv:1003.3101 [astro-ph.GA]].

[17] B. Feldstein, A. L. Fitzpatrick and E. Katz, JCAP **1001**, 020 (2010) [arXiv:0908.2991 [hep-ph]].

[18] E. Komatsu *et al.* [WMAP Collaboration], Astrophys. J. Suppl. **180**, 330 (2009) [arXiv:0803.0547 [astro-ph]].

[19] E. Aprile *et al.* [XENON100 Collaboration], Phys. Rev. Lett. **107**, 131302 (2011) [arXiv:1104.2549 [astro-ph.CO]].

[20] E. Aprile *et al.* [XENON100 Collaboration], arXiv:1207.5988 [astro-ph.CO].

[21] E. Aprile *et al.* [XENON100 Collaboration], Astropart. Phys. **35**, 573 (2012) [arXiv:1107.2155 [astro-ph.IM]].

[22] E. Aprile *et al.*, Phys. Rev. Lett. **97**, 081302 (2006) [astro-ph/0601552].

[23] E. Aprile, talk given at UCLA Dark Matter 2012, `https://hepconf.physics.ucla.edu/dm12/talks/aprile.pdf`.

[24] K. Schmidt-Hoberg and M. W. Winkler, JCAP **0909**, 010 (2009) [arXiv:0907.3940 [astro-ph.CO]].

[25] Z. Ahmed *et al.* [CDMS Collaboration], Phys. Rev. Lett. **102**, 011301 (2009) [arXiv:0802.3530 [astro-ph]].

[26] Z. Ahmed *et al.* [CDMS-II Collaboration], Science **327**, 1619 (2010) [arXiv:0912.3592 [astro-ph.CO]].

[27] Z. Ahmed *et al.* [CDMS-II Collaboration], Phys. Rev. Lett. **106**, 131302 (2011) [arXiv:1011.2482 [astro-ph.CO]].

[28] K. R. Dienes, J. Kumar and B. Thomas, "Dynamical Dark Matter: Direct Detection and Experimental Uncertainties," to appear.

[29] T. Han and R. Hempfling, Phys. Lett. **B415**, 161 (1997) [arXiv:hep-ph/9708264];
      L. J. Hall, T. Moroi and H. Murayama, Phys. Lett. **B424**, 305 (1998) [arXiv:hep-ph/9712515].

[30] D. Tucker-Smith and N. Weiner, Phys. Rev. D **64**, 043502 (2001) [arXiv:hep-ph/0101138]; Phys. Rev. D **72**, 063509 (2005) [hep-ph/0402065].

[31] K. Kumar, A. Menon and T. M. P. Tait, arXiv:1111.2336 [hep-ph].

[32] K. R. Dienes, J. Kumar and B. Thomas, "Inelastic Scattering of Dynamical Dark Matter," to appear.